Molecular Therapy
Methods & Clinical Development
Original Article

Large-scale manufacturing of base-edited chimeric antigen receptor T cells

Rosie Woodruff,[1] Farhaan Parekh,[1] Katarina Lamb,[1] Leila Mekkaoui,[1] Christopher Allen,[1] Katerina Smetanova,[2] Jasmine Huang,[2] Alex Williams,[1] Gerardo Santiago Toledo,[1] Koki Lilova,[1] Claire Roddie,[3] James Sillibourne,[1] and Martin Pule[1,3]

[1]Autolus Therapeutics, The Mediaworks, 191 Wood Lane, W12 7FP London, UK; [2]Imperial College London, South Kensington Campus, SW7 2AZ London, UK; [3]Deparment of Haematology, Cancer Institute, 72 Huntley Street, WC1E 6BT London, UK

Base editing is a revolutionary gene-editing technique enabling the introduction of point mutations into the genome without generating detrimental DNA double-stranded breaks. Base-editing enzymes are commonly delivered in the form of modified linear messenger RNA (mRNA) that is costly to produce. Here, we address this problem by developing a simple protocol for manufacturing base-edited cells using circular RNA (circRNA), which is less expensive to synthesize. Compared with linear mRNA, higher editing efficiencies were achieved with circRNA, enabling an 8-fold reduction in the amount of RNA required. We used this protocol to manufacture a clinical dose (1×10^8 cells) of base-edited chimeric antigen receptor (CAR) T cells lacking expression of the inhibitory receptor, PD-1. Editing efficiencies of up to 86% were obtained using 0.25 μg circRNA/1×10^6 cells. Increased editing efficiencies with circRNA were attributed to more efficient translation. These results suggest that circRNA, which is less expensive to produce than linear mRNA, is a viable option for reducing the cost of manufacturing base-edited cells at scale.

INTRODUCTION

Cell engineering is revolutionizing the treatment of genetic diseases, autoimmune disorders, and cancers. The advent of early gene-editing tools, such as transcription factor-like endonucleases (TALENS), zinc finger nucleases, and clustered regularly interspaced short palindromic repeats (CRISPR)-CRISPR-associated nuclease 9 (Cas9), has greatly extended the possibilities of cell therapies by enabling the disruption of genes[1–5] and targeted gene insertion.[6–11] These approaches rely on the formation of DNA double-stranded breaks, which are predominantly repaired by non-homologous end-joining to introduce insertions or deletions that disrupt gene expression, or alternatively by homology-directed repair to mediate gene integration. However, particularly when multiplexing, gene editing can result in aneuploidy, chromosomal translocations, and significant genotoxicity.[1,12–15]

Base editing is an alternative method that uses enzymes to modify DNA without generating DNA double-stranded breaks, thus reducing the likelihood of translocations.[16–18] Base editing involves directing a deaminase domain, via a DNA-binding domain, to a specific site in the genome where it modifies target bases to either introduce[19–21] or correct mutations.[22–24] Early base editors fused Cas9 nickase (Cas9n) to a deaminase domain, with targeting being mediated by the guide RNA (gRNA) to which Cas9n binds. Adenine and cytosine deaminase domains, which convert adenosine to guanosine (A to G)[25,26] and cytidine to thymidine (C to T)[27] in DNA, respectively, have been mutated to alter their specificity or to reduce off-target editing.[28–30]

Base editor technology is rapidly advancing the field of cell and gene therapies. The correction of pathogenic mutations is a promising strategy for the treatment of genetic diseases, including sickle cell anemia,[24] β-thalassaemia,[31] Hutchinson-Gilford progeria syndrome,[22] spinal muscular atrophy,[32] and familial hypercholesterolemia.[33,34] Base editors are also being employed to facilitate precise gene disruption through the introduction of stop codons or perturbation of mRNA splicing.[18,21] This approach is being adopted for the production of allogeneic chimeric antigen receptor (CAR) T cell therapies.[17,35] The results of a first-in-human clinical trial have been recently reported for three T-ALL patients receiving anti-CD7 CAR T cells engineered with disruptive edits of the *TRBC*, *CD7*, and *CD52* genes.[36] Despite reports of multilineage cytopenia, the results support further investigation of base-edited CAR T products.[36]

Approaches to delivering base-editing enzymes include mRNA or ribonucleic protein (RNP) complex transfection,[31,37] and transduction with adeno-associated virus (AAV).[18,32] Messenger RNA delivery is the favored approach due to challenges with purifying the base editor protein[37] and the cost of producing AAV. While mRNA transfection is the most widely adopted approach,[17,35,36] modifications are required to introduce stabilizing elements such as a 5′ 7-methylguanylate cap and a 3′ poly adenylated [poly(A)] tail. Modified nucleosides may also be incorporated to reduce degradation.[38,39] For clinical applications, large quantities of high-purity capped and tailed mRNA are required. The expense of producing linear mRNA is currently a barrier

Received 15 August 2023; accepted 29 September 2023;
https://doi.org/10.1016/j.omtm.2023.101123.

Correspondence: Martin Pule, Autolus Therapeutics, The Mediaworks, 191 Wood Lane, W12 7FP London, UK.
E-mail: m.pule@autolus.com

to clinical application of base editing. Approaches that simplify mRNA production and/or result in a lower requirement are hence desirable.

The use of circular RNA (circRNA), where the 5′ and 3′ ends of the molecule are covalently joined, not only circumvents the requirement for the RNA to be capped and poly(A) tailed, but also offers increased stability due to exonuclease resistance. Several methods exist for generating circRNA,[40–42] but the most frequently used is permuted intron-exon (PIE) self-splicing RNAs,[43–45] which promote back-splicing to facilitate circularization. Through the inclusion of an internal ribosome entry site (IRES), it is possible to direct translation of coding sequences from circRNAs and achieve higher levels of expression compared with linear mRNA.[41,46,47] Here, we explored the utility of circRNA encoding the cytosine base editor, BE4max, for large-scale base-editing. We compared the stability and efficacy of linear and circular BE4max RNA for base editing-induced disruption of TIM3 and PD-1 expression. We also demonstrated application of circular base editor RNA in a semi-closed manufacturing protocol for the large-scale production of base-edited CAR T cells.

RESULTS

RNA encoding the cytosine base editor BE4max can be circularized

We first sought to determine if a PIE self-splicing RNA strategy could efficiently circularize RNA encoding BE4max, which has a relatively long coding sequence. BE4max was cloned into a plasmid containing the PIE sequence from the group I intron of *Anabaena* pre-tRNA[45,46] (Figure 1A). A linear RNA template with 5′ and 3′ untranslated regions (UTRs) and a poly(A) signal sequence was also generated as a control (Figure 1A). RNAs were synthesized by *in vitro* transcription (IVT) and circRNA produced by promoting back-splicing; while linear RNA was capped, and poly(A) tailed (Figures 1B and 1C).

Fractionation of the linear mRNA on a bioanalyzer indicated that it was of the expected length of 5,990 bases (Figure 1D). Analysis of the circRNA indicated faster migration after circularization, consistent with its shorter length of 6,497 bases (Figure 1D, left lane). Bands corresponding to the size of the released introns (5′ intron, 624 bases and 3′ intron, 181 bases) were also present (Figure 1D, right lane). A circularization efficiency of 68.7% was determined from bioanalyzer data (Figure 1E).

To confirm circularization, the circRNA was reverse transcribed and the region spanning the exon 1 and exon 2 splice site amplified by PCR and Sanger sequenced. This clearly demonstrated that the exons were fused, and the RNA was circular (Figure 1F). Together, these data demonstrate the feasibility of producing circRNA encoding BE4-max from *in vitro* transcribed RNA using the self-splicing *Anabaena* pre-tRNA PIE sequence.

Enhanced BE4max expression from circRNA

Next, we explored BE4max expression from circRNA in primary human T cells. $CD4^+/CD8^+$ sorted T cells were nucleofected with 4.00 μg RNA/1 × 10^6 cells of linear or circRNA. Cellular lysates were prepared from the 24-, 48-, 72-, and 96-h samples and western blotting carried out with an anti-Cas9 antibody mix to enable BE4max detection (Figures 2A and S1A). The BE4max protein (212.6 kDa) was detectable 24 h after nucleofection with circRNA, followed by a gradual decrease in expression over the course of 72 h (Figures 2A and S1A). On the other hand, the BE4max expression from linear mRNA was significantly lower and was below the limit of detection in one donor (Figure S1A, top panel). As cells were nucleofected with comparable amounts of RNA, these results suggest a higher translational capacity of circRNA than linear mRNA. To determine whether RNA stability was a contributing factor, we investigated the rate of RNA decay in nucleofected T cells.

To determine the rate of RNA degradation, RNA was extracted from cells within the first 2 h and then at 24-, 48-, 72-, and 96-h post-nucleofection. RT-qPCR was carried out to quantify transcript copy numbers of the BE4max base editor along with the housekeeping gene, glyceraldehyde-3-phosphate dehydrogenase (GAPDH) (Figures 2B, S1B, and S1C). BE4max transcript copy numbers were normalized to GAPDH, and RNA decay was determined by further normalization to the initial starting time point. These data revealed similar rates of decay for BE4max linear and circRNA, with ∼90% of RNA degradation occurring within the first 24 h (Figure 2B). Reducing the RNA amount from 4.00 μg to 0.25 μg RNA/1 × 10^6 cells did not appear to affect the kinetics of decay (Figures 2B, S1B, and S1C).

CircRNA efficiently directs base editing in primary human T cells

To compare base-editing efficiencies obtained using linear or circular RNA, stimulated peripheral blood mononuclear cells (PBMCs) were nucleofected with BE4max RNA and a non-targeting or a targeting single guide RNA (sgRNA) directed to the T cell inhibitory receptors, TIM3 (*HAVCR2*) or PD-1 (*PDCD1*) (Figures 3A and 3B). PBMCs from five or three donors were nucleofected with increasing amounts of linear or circular RNA, ranging from 0.25 μg to 4.00 μg RNA/1 × 10^6 cells and a fixed amount of sgRNA (30 pmol/1 × 10^6 cells). After 4 days, T cells were restimulated to up-regulate the expression of the target genes and the following day, surface expression was determined (Figures 3A and 3B, bottom panels).

Successful *HAVCR2* editing was demonstrated with 4.00 μg RNA/1 × 10^6 cells of circular and linear RNA by a decrease in the mean percentage of $TIM3^+$ T cells to 10.3% and 20.1%, compared with 76.6% and 75.7% in the non-targeting control samples, respectively (Figure 3C). In T cells receiving 0.25 μg, 0.50 μg, 1.00 μg, and 2.00 μg circRNA/1 × 10^6 cells, the mean percentage of $TIM3^+$ T cells was reduced to 31.1%, 19.1%, 14.6%, and 10.9%, respectively (Figure 3C). Beyond 2.00 μg circRNA/1 × 10^6 cells, no further decrease in $TIM3^+$ T cells was observed (Figure 3C). As 0.50 μg of circRNA and 4.00 μg of linear mRNA resulted in similar reductions of $TIM3^+$ T cells (19.1% and 20.1%, respectively), approximately eight times less circRNA was required for efficient base editing (Figure 3C).

PDCD1 gene disruption was also explored using previously described guides (Figure 3B).[18] The mean percentage of $PD\text{-}1^+$ T cells was

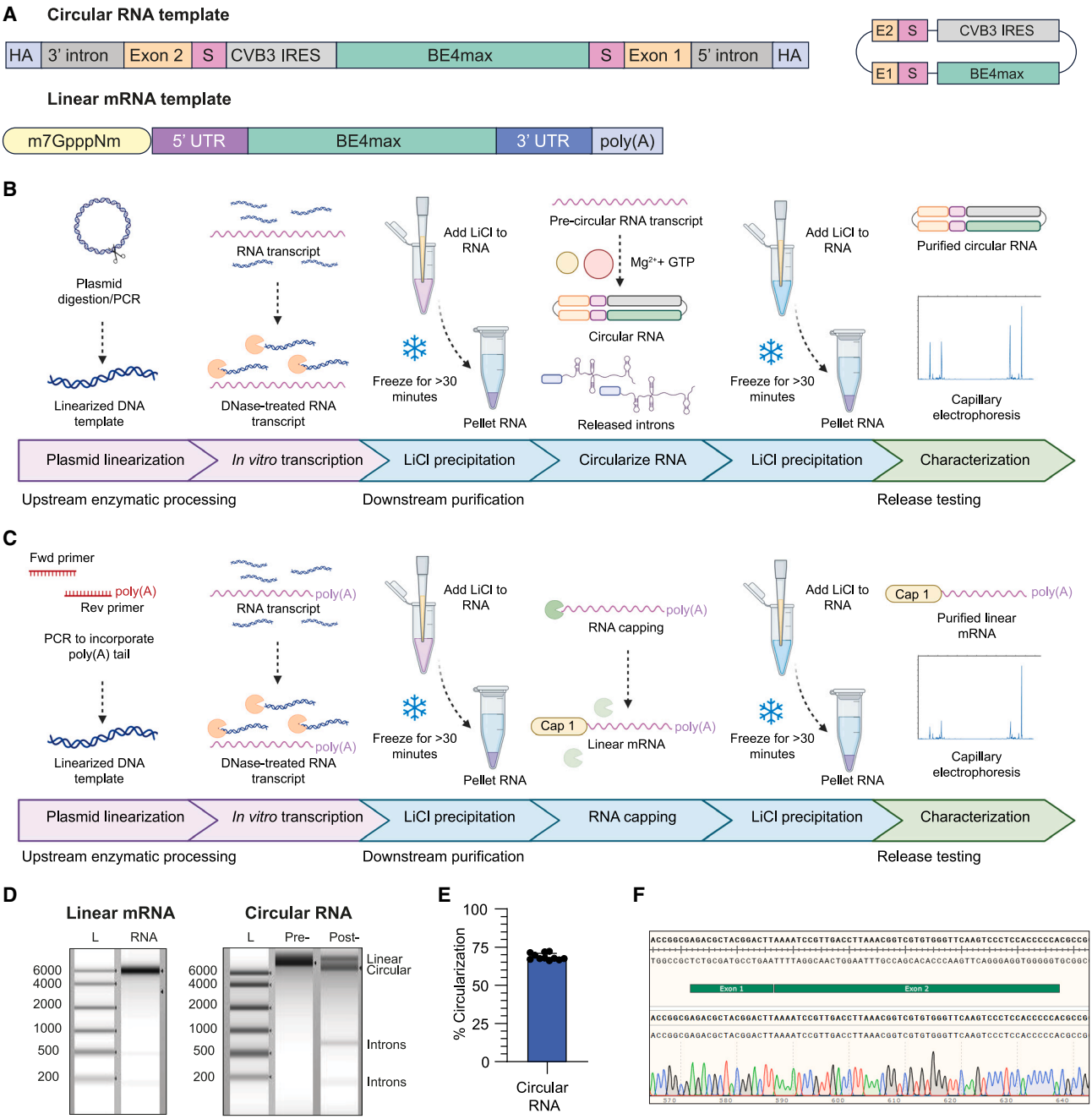

Figure 1. Generation of RNAs encoding the cytosine base editor

Production of BE4max RNA. (A) Structure of the IVT templates used to generate circular (top) and linear (bottom) RNA encoding the cytosine base editor, BE4max. CircRNA was generated using the *Anabaena* pre-tRNA PIE sequence. Complementary homology arms (HA) flanking the PIE sequence promote back-splicing, while spacer sequences (S) facilitate splicing bubble formation to produce circRNA. An internal ribosome entry site (IRES) derived from coxsackievirus B3 (CVB3) initiates translation. Linear BE4max RNA with 5′ and 3′ untranslated regions (UTRs) was poly(A) tailed and enzymatically capped and methylated (m7GpppNm) to generate Cap 1 mRNA. (B and C) Flow diagrams showing the synthesis of circular (B) and linear (C) RNA. (D) TapeStation bioanalyzer analysis of linear and circular RNA to verify transcript size and integrity. (E) Circularization efficiency as determined by measuring peak height on the TapeStation bioanalyzer, calculated as a proportion of full-length RNA. Data are mean ± standard deviation of 11 independent runs. (F) Electropherogram showing the sequence of fused exons in the circRNA.

56.0% and 63.2% in the non-targeting control samples and 10.7% and 10.1% in those receiving the PD-1 sgRNA and 4.00 μg RNA/1 × 10^6 cells of circular or linear RNA, respectively (Figure 3D). Although disruption was similar at 4.00 μg RNA/1 × 10^6 cells, when the RNA amount was titrated down to 2.00 μg, 1.00 μg, 0.50 μg, and 0.25 μg RNA/1 × 10^6 cells, circRNA was more efficient at disrupting *PDCD1* than linear mRNA. The mean percentage of PD-1^+ T cells was reduced to 8%, 4.2%, 15.6%, and 19.9% using circRNA, compared with 20.0%, 31.6%, 43.3%, and 52.1% using linear mRNA, respectively (Figure 3D). Some donor-to-donor variability in *PDCD1* editing efficiency was observed, depending on which species of RNA was used. The underlying cause of this variability remains to be determined but may reflect differences between the donors in the rate of translation or turnover of the circular and linear RNA. Overall, these data indicate that BE4max circRNA can disrupt the expression of T cell inhibitory receptors more efficiently than linear mRNA.

Efficient base conversion using circRNA is confirmed by sequencing

To confirm base editing at the genomic level, genotyping was performed by amplifying across the target site, followed by Sanger sequencing of the PCR product and determining on-target and bystander base conversion efficiencies using EditR.[48] At the *HAVCR2* target site, a positive correlation was observed between the amount of RNA and the editing efficiency, with the highest frequency of base conversion occurring at the splice acceptor site (C6 in the base-editing window) and the bystander position at C5 (Figures 4A, 4C, and S2A). Near complete base conversion was observed in all donors edited with 4.00 μg and 2.00 μg circRNA/1 × 10^6 cells (Figures 4A and 4C). Using 1.00 μg, 0.50 μg, and 0.25 μg RNA/1 × 10^6 cells, circRNA resulted in 91%, 76%, and 58% on-target editing, compared with 58%, 43%, and 25% with linear mRNA, respectively (Figure 4C). CircRNA facilitated greater on-target editing than linear mRNA, most notably at the lower RNA amounts.

Similarly, genotyping was performed on the PD-1 edited samples to determine the frequency of cytosine conversion within the base-editing window (Figures 4B, 4D, and S2B). Cytosines were predominantly converted to thymines, although other base substitutions, including adenine and guanine, were also observed at lower frequencies (Figure 4B). Overall, the highest level of target cytosine conversion in the splice donor site (C7 in the base-editing window) was obtained using circRNA, with 1.00 μg RNA/1 × 10^6 cells yielding nearly 100% conversion rates, substantially higher than the 44% and 80% editing with 1.00 μg and 4.00 μg linear mRNA/1 × 10^6 cells, respectively (Figure 4D). These results indicate more efficient on-target editing with circRNA than linear mRNA.

Large-scale manufacturing of base-edited CAR T cells using circRNA

We next tested circRNA-mediated base editing in a large-scale CAR T manufacturing process (Figure 5A). $CD4^+$/$CD8^+$ cells were isolated from leukapheresate using the CliniMACS Prodigy and activated for 2 days prior to nucleofection with BE4max circRNA and either

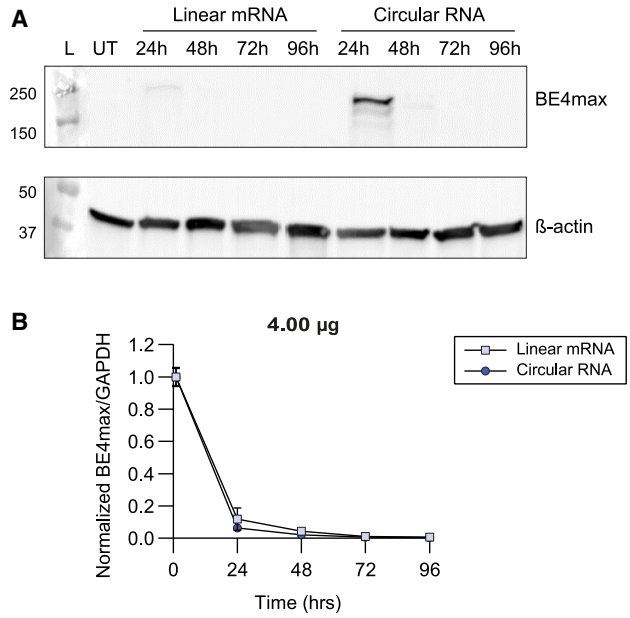

Figure 2. Enhanced translation of the cytosine base editor from circRNA

BE4max protein expression and rate of linear or circular RNA degradation in T cells nucleofected with 4.00 μg RNA/1 × 10^6 cells. (A) Western blotting for BE4max using antibodies recognizing Cas9 and β-actin (loading control). Substantially higher levels of BE4max translation were observed from circRNA compared with linear mRNA. The blots were prepared from samples collected at 24, 48, 72, and 96 h post-nucleofection. (B) BE4max and GAPDH RT-qPCR results from samples collected within the first 2 h of nucleofection and then at 24, 48, 72, and 96 h post-nucleofection. The BE4max/GAPDH copy number ratio was calculated and normalized to the first time point to determine the rate of RNA decay. Both linear and circular RNA decayed at the same rate, with ∼90% of the RNA being degraded within 24 h. The data represent the mean ± standard deviation of triplicate RT-qPCR results from three healthy donors. Where there was no variation in the data, the error bars were omitted.

the PD-1 or non-targeting sgRNA. Two different amounts of circRNA, 0.25 μg and 1.00 μg RNA/1 × 10^6 cells, were tested in three healthy donors each. The nucleofected T cells were transduced with lentiviral vector containing an anti-CD19 CAR[49–52] on day 3 (Figures 5A, 5B, S3, and S4) and transduced and non-transduced T cells were cultured for 9 days before cryopreservation (Figure 5A).

No differences in transduction efficiency or expansion were observed between the different amounts of circRNA and the non-targeting or PD-1 sgRNA (Figures S3, S4A, and S4C). Edited CAR T cells expanded approximately 2- to 3-fold to achieve ∼1 × 10^8 cells from ∼5 × 10^6 nucleofected cells, with similar viabilities to the no pulse control cells by day 9 (Figure S4C; Tables S1–S4). The exhaustion profiles of non-targeting-edited or PD-1-edited cells on day 9 were as follows: few PD-1^+ T cells were observed across all samples, the $TIM3^+$ population was generally lower in donors edited with 0.25 μg circRNA/1 × 10^6 cells compared with 1.00 μg circRNA/1 × 10^6 cells, and the percentage of $LAG3^+$ T cells was comparable across all samples and the amount of RNA (Figure S5).

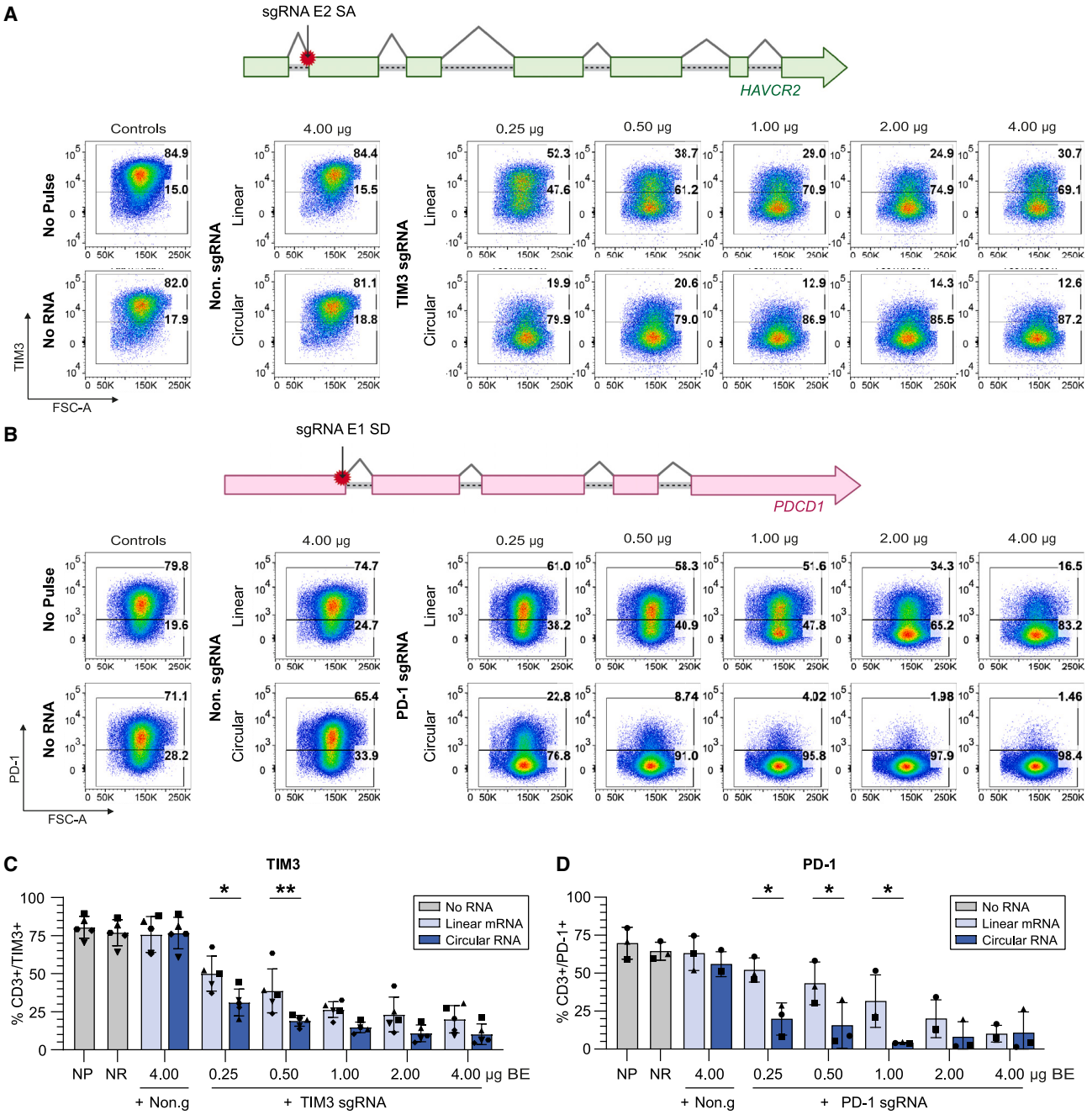

Figure 3. Phenotyping of base-edited T cells using increasing amounts of linear or circular RNA

CircRNA is more efficient than linear mRNA for base editing. (A and B) Base editing of the T cell inhibitory receptors, TIM3 (*HAVCR2*) (A) or PD-1 (*PDCD1*) (B), using increasing amounts of linear or circular BE4max RNA and a targeting or non-targeting (Non.) sgRNA. The location of the sgRNA is shown on the gene target (top panel), and flow cytometric analysis of restimulated T cells stained with antibodies to CD3 and TIM3 or PD-1 on day 7 is shown for a single representative donor for each target (bottom panel). (C and D) Quantification of $CD3^+/TIM3^+$ (C) or $CD3^+/PD\text{-}1^+$ (D) T cells on day 7 following 24 h of restimulation, represented as mean ± standard deviation of five (TIM3) or three (PD-1) donors (shown as different symbols within each graph). Robust editing was observed in cells nucleofected with circRNA, with the lowest amount of RNA, 0.25 µg RNA/1×10^6 cells, the percentage of $TIM3^+$ T cells was reduced to ~30% on average and the percentage of $PD\text{-}1^+$ T cells was reduced to ~20% on average. A greater reduction in $TIM3^+$ and $PD\text{-}1^+$ T cells was observed with circRNA than linear mRNA (TIM3, 0.25 µg, $p = 0.0115$, 0.50 µg, $p = 0.0081$; PD-1, 0.25 µg, $p = 0.0151$, 0.50 µg, $p = 0.0439$, 1.00 µg, $p = 0.0457$). Two-way ANOVA; $^*p \leq 0.05$, $^{**}p \leq 0.01$. No pulse (NP), No RNA (NR).

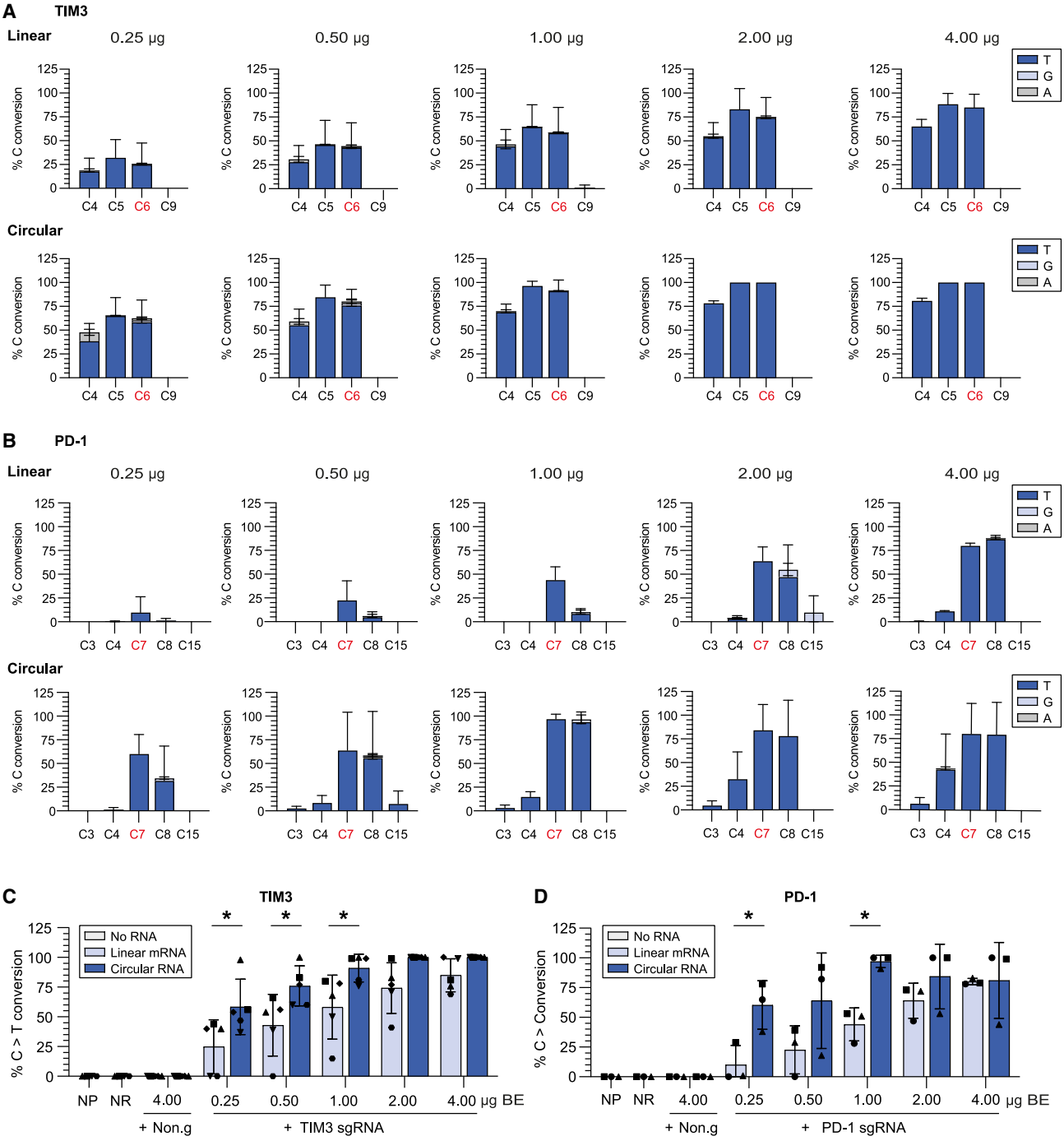

Figure 4. Genotyping of base-edited T cells reveals higher editing efficiencies using circRNA

Cytosine base conversion efficiencies were determined by genotyping and EditR analysis. (A and B) All cytosines within the TIM3 (*HAVCR2*) (A) and PD-1 (*PDCD1*) (B) protospacer sequences were examined for C > T base conversion, as well as C > A and C > G mutations, represented as mean ± standard deviation. The target cytosine, corresponding to the essential guanine in the splicing site, is indicated in red. Cytosines that did not show any editing were excluded from the graph. Higher C > T conversion efficiencies were obtained with the BE4max circRNA at all RNA amounts. (C and D) C > T conversion efficiency at the corresponding target cytosine, C6 for TIM3 (C) and C7 for PD-1 (D), showing more efficient conversion after editing with BE4max circRNA (TIM3, 0.25 µg, $p = 0.0356$, 0.50 µg, $p = 0.0405$, 1.00 µg, $p = 0.0422$; PD-1, 1.00 µg, $p = 0.0410$). The data represent the mean ± standard deviation from five donors for TIM3 and three donors for PD-1 (shown as different symbols within each graph). Where there was no variation in the data, the error bars were omitted. Two-way ANOVA; *$p \leq 0.05$. NP, no pulse; NR, no RNA.

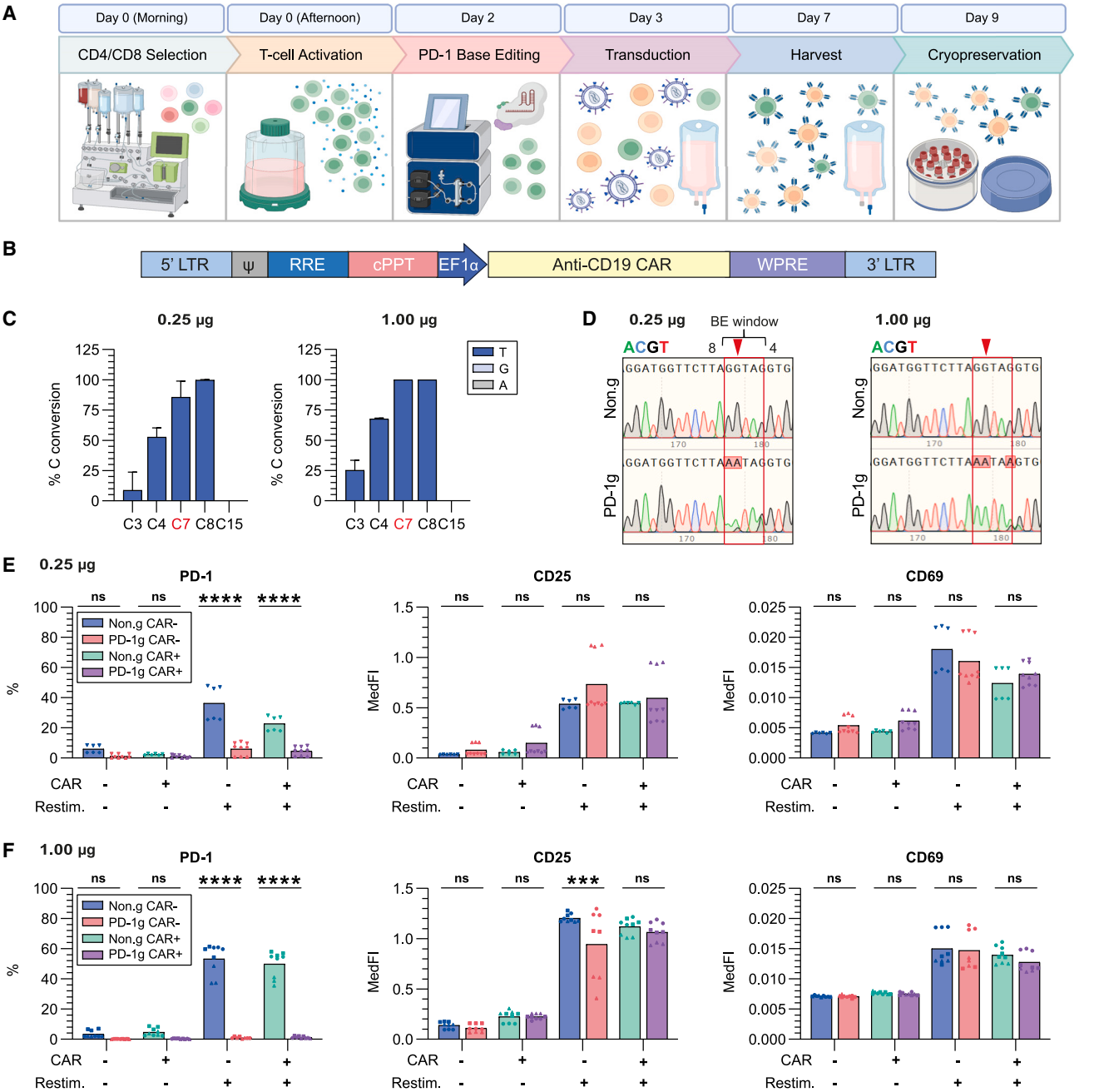

Figure 5. Large-scale manufacturing of base-edited CAR T cells

Efficiency of circRNA for manufacturing PD-1 edited CAR T cells. (A) Diagram illustrating the large-scale manufacturing process. (B) Schematic of the anti-CD19 CAR vector used to transduce T cells. LTR, long terminal repeat; RRE, Rev-responsive element; cPPT, central polypurine tract; EF1α, elongation factor 1 α promoter region; CAR, chimeric antigen receptor; WPRE, woodchuck hepatitis virus post-transcriptional regulatory element. (C) Percent cytosine conversion (mean ± standard deviation of three donors) across the protospacer, as determined by genotyping and EditR analysis from day 9 samples, showing 86% and 100% C > T conversion at the C7 target cytosine using 0.25 µg or 1.00 µg circRNA/1 × 10^6 cells, respectively. Cytosines that did not show any editing were excluded from the graph. Where there was no variation in the data, the error bars were omitted. (D) Electropherograms showing on-target base conversion of the guanine of the splice donor site (marked with red arrowhead), achieved by editing the C7 target cytosine on the antisense strand, and G > A conversion of the guanine occurring at the adjacent position (C8). (E and F) T cells base-edited using 0.25 µg (E) or 1.00 µg (F) circRNA/1 × 10^6 cells were cryopreserved on day 9 and upon thawing were restimulated with TransAct for 24 h. Activation marker expression was determined by flow cytometry, shown as percent PD-1^+ cells (left), or median fluorescence intensity of CD25 (middle) or CD69 (right) expression (normalized to CountBright

(legend continued on next page)

The efficiency of PD-1 editing was determined by carrying out EditR analysis (Figures 5C and 5D). Although no editing was detected with the non-targeting sgRNA, the PD-1 sgRNA resulted in near complete conversion of the target cytosine (C7 in the editing window) to thymine in all three donors, as well as the adjacent bystander cytosine (C8) when nucleofected with 1.00 μg circRNA/1 × 10^6 cells (Figure 5C, right). Base editing with 0.25 μg circRNA/1 × 10^6 cells was slightly less efficient, with a lower on-target conversion rate of 86% (Figure 5C, left). Bystander editing was observed within the editing window (C4 and C8), as well as immediately outside (C3) (Figures 5C and 5D); however, no other base conversions were observed within the protospacer sequence.

To confirm that editing of the PD-1 exon 1 splice donor site resulted in loss of protein expression, T cells were restimulated with TransAct for 24 h and stained with antibodies against the inhibitory receptor, PD-1, and activation markers, CD25 (IL-2Rα) and CD69 (Figures 5E and 5F). Although restimulation resulted in PD-1 upregulation in all treated samples, the population of PD-1^+ T cells was significantly reduced in all PD-1-edited samples. Upregulation of CD25 and CD69 was observed in all restimulated samples regardless of the editing process (Figures 5E and 5F). T cells edited with 0.25 μg circRNA/1 × 10^6 cells and the non-targeting or PD-1 sgRNA had mean PD-1^+ populations of 22.8% and 4.7%, respectively (Figure 5E). For 1.00 μg circRNA/1 × 10^6 cells, the percentage of PD-1^+ T cells was ∼2% in the edited sample compared with 49.9% in the non-targeting control sample, whereas CD25 and CD69 were upregulated in both (Figure 5F). These results demonstrate that 0.25 μg circRNA/1 × 10^6 cells is an amount sufficient to disrupt gene expression in T cells at large scale.

DISCUSSION

The large-scale manufacture of base-edited cellular therapies is limited by the complexity and cost of producing long RNA transcripts encoding the base editor enzyme at sufficient quality and scale. Linear mRNA manufacturing requires multiple steps to modify the transcript to incorporate a 5′ 7-methylguanylate cap and a 3′ poly(A) tail. The capping process can either be performed using post-transcriptional capping enzymes, which generates a pool of capped and uncapped transcripts; or by co-transcriptional methods using cap analogs, such as the anti-reverse cap analog (Cap 0)[53] and the Cap 1 analogs.[54] In addition to the 5′ cap, linear mRNA requires a 3′ poly(A) tail to promote its stability.[55] The poly(A) tail can be incorporated either into the DNA template by the addition of thymine bases in the reverse primer, or added post-transcriptionally using enzymatic methods that rely on the poly(A) polymerase. The scalability of linear mRNA manufacturing is limited by the high cost of capping and tailing reagents, as well as the requirement to purify the RNA before and after modification, which can result in a loss of mRNA yield.

An alternative to linear mRNA is circRNA, which is modified in its structure as the 5′ and 3′ ends of the transcript are covalently closed. CircRNA is potentially advantageous compared with linear mRNA, as it does not require capping or polyadenylation, thereby reducing manufacturing costs. CircRNA can be generated by back-splicing and several PIE self-splicing RNAs have been described, including the group I intron from an *Anabaena* tRNA,[45,46] *Tetrahymena thermophila*[44,45,56] and bacteriophage T4 thymidylate synthase.[57] CircRNAs have received increasing interest in the biotechnology field due to their diverse functions. These RNAs can act as aptamers to manipulate cellular functions,[58,59] as therapeutic agents to sponge disease-related microRNAs[60,61] or proteins,[62] or as immunological agents for vaccination.[63] Although circRNA has not been described for base-editing purposes, Liu et al. report their use to enhance prime editing efficiencies.[64]

The process of generating circRNA is simple and involves IVT of the self-splicing sequence, followed by heating the transcript in a circularization buffer containing magnesium ions and guanosine triphosphate, which initiates the back-splicing process to ligate the exons and release the intronic sequences. Although RNA circularization efficiency is dependent on the transcript length, with longer RNAs being less efficiently circularized than short RNAs,[46] we found that circRNA encoding the long base editors (∼6.4 kb) can be efficiently generated *in vitro* using the *Anabaena* PIE self-splicing pre-tRNA,[46] with a mean circularization efficiency of 68.7%. CircRNA can be purified by lithium chloride precipitation to allow removal of the buffer contaminants while retaining the RNA integrity, unlike column-based approaches, which were found to cause degradation of the transcript (data not shown). Compared with the production of linear mRNA, circRNA offers a simple and streamlined manufacturing process with significantly lower production costs.

As previous studies have reported the improved half-life and translational capacity of circRNAs,[46,65–67] we monitored the stability of BE4max-encoding linear and circular RNA in T cells. Surprisingly, RT-qPCR results revealed that linear and circular RNAs decay at a comparable rate; however, circRNA resulted in increased protein production within 24 h of RNA transfection, which led to a prolonged duration of BE4max expression (∼48 h). Unlike linear mRNA, translation from circRNAs occurs in a cap-independent manner and initiates from the IRES and terminates at the stop codon at the 3′ end of the transcript. Polyadenosyl-binding proteins interact with the cap and poly(A) tail of linear mRNA to promote RNA stability and translation initiation,[55] and the closed structure of circRNA may

beads). The data represent the mean of triplicate samples from three donors for each group (shown as different symbols). Two donors are shown for the non-targeting edited samples at the lower RNA amount, as the control sample for one donor was edited using 1.00 μg circRNA/1 × 10^6 cells only. Compared with the non-edited cells, the PD-1 sgRNA resulted in a reduction in PD-1^+ cells after stimulation (0.25 μg, CAR−/+ $p < 0.0001$; 1.00 μg, CAR−/+ $p < 0.0001$) and a reduction in CD25 expression in the non-transduced cells of the 1.00 μg circRNA/1 × 10^6 cells group (CD25, CAR-p = 0.0004). Two-way ANOVA; ns, $p > 0.05$, *$p \leq 0.05$, ***$p \leq 0.001$, ****$p \leq 0.0001$.

aid ribosome recruitment and continuous translation in an analogous manner. Western blotting results supported higher translational activity from the circRNA than the linear RNA.

Consistent with higher translational activity from the circRNA, it was found from titration of the RNA amount in small-scale experiments that less circRNA was required for efficient editing; although donor-specific variability was observed, the RNA amount could be reduced by approximately 8-fold. These results were confirmed by flow cytometric analysis and genomic sequencing of TIM3 and PD-1 base-edited T cells. Large-scale experiments using 0.25 μg circRNA/1 × 10^6 cells supported these data and clearly demonstrated that less circRNA was required for near complete editing of *PDCD1*.

To demonstrate scalability of the protocol, we combined base editing of a clinically relevant gene target with the introduction of an anti-CD19 CAR, aiming to manufacture 1 × 10^8 base-edited CAR T cells. Using $CD4^+$/$CD8^+$ sorted T cells and 1.00 μg circRNA/ 1 × 10^6 cells, we achieved near complete base conversion at the target splice site at the *PDCD1* loci. As the PD-1 sgRNA sequence had been previously validated,[18] we did not assess the off-target events in our study. Cas9-dependent off-target editing may be minimized by careful gRNA selection to reduce mismatches with the target sequence. Off-target sites may be predicted using computational tools,[68] and the type and frequency of off-target edits can be determined by sequencing methods, such as DiGenome-seq,[69,70] GUIDE-seq,[71] Detect-seq,[72] or whole genome sequencing. Off-target deamination may also occur in a Cas9-independent manner, and the choice of base editor and delivery method may reduce such events.[73–76]

The base-edited T cells were transduced with lentivirus 1 day after nucleofection, and the disruption of PD-1 did not impact the transduction efficiency, with approximately 60% of T cells expressing the CAR. Although a drop in cell number was observed 1 day after nucleofection, the T cells recovered and expanded to meet the dose requirements (1 × 10^8 CAR T cells) by day 9. By transducing the cells after nucleofection, we were able to reduce the vector requirements compared with transducing the T cells prior to nucleofection. As 100% base conversion was observed in $CD4^+$/$CD8^+$ sorted donors, we set out to reduce the RNA amount by a further 4-fold. By reducing the amount to 0.25 μg circRNA/1 × 10^6 cells we could achieve 86% base conversion, while maintaining high transduction efficiencies and comparable expansion profiles in PD-1-edited and non-targeting-edited CAR T cells.

CircRNA has a simplified manufacturing workflow, and increased editing efficiencies owing to its high efficiency of translation. To scale the production of circRNA for clinical use, ∼12.5 μg RNA is required for nucleofection of 5 × 10^7 $CD4^+$/$CD8^+$ sorted T cells, to achieve ∼1 × 10^8 edited CAR T cells at the end of the culture. Unlike linear mRNA, circRNA does not require verification of capping and polyadenylation; instead, circularization must be confirmed by sequencing the cDNA across the back-splicing junction. CircRNA can be easily distinguished from linear molecules by capillary electrophoresis, due to its reduced size after the release of the intronic sequences. As some linear RNA and intronic sequences remain after circularization, previous reports have treated circRNA with RNase R.[66] However, linear RNA digestion is not always complete and RNase R digestion can reduce the yield of circRNA[66] due to nicking of the transcript.[77]

CircRNA may be further improved, as the inclusion of 5′ and 3′ UTR sequences have been found to enhance the translation of circRNA produced using the T4 thymidylate synthase intron.[47] Furthermore, the IRES can be engineered with synthetic aptamers to recruit translation initiation machinery.[47] Linear mRNA benefits from the incorporation of modified nucleosides, such as pseudouridine, N^1-methylpseuodouridine, 5-methylcytidine, and N^6-methyladenosine, to reduce its immunogenicity by preventing signaling through Toll-like receptors.[78–80] Some nucleoside modifications can disrupt back-splicing of PIE sequences,[66] but 5% N^6-methyladenosine can be incorporated into the bacteriophage T4 thymidylate synthase PIE to increase its stability through resistance to nuclease digestion.[47] Optimization of the sgRNA amount for co-delivery with circRNA may further enhance the editing efficiencies, by ensuring sgRNA availability for pairing with the base editor protein. Alternative methods of circRNA transfection may improve the quality of engineered cells, as well as enabling closed and automated manufacturing. Although nucleofection results in a high efficiency of transfection, the high-voltage pulses and serum-free electroporation buffers can cause cell death.[81] Recently, the development of mRNA-encapsulated lipid nanoparticles has revolutionized the field of RNA therapeutics and may be simpler and cause less cell loss than electroporation.

In summary, we demonstrate the application of circRNA for base editing in primary T cells and prove that it is superior to linear mRNA. Our approach can be scaled to manufacture ∼1 × 10^8 base-edited anti-CD19 CAR T cells with near complete gene disruption. This process could be scaled up to engineer cells for autologous and allogeneic cell therapies. By streamlining circRNA production and reducing the amount of RNA for efficient editing, the cost of base-edited cell therapies can be significantly reduced.

MATERIALS AND METHODS

Cell lines

HEK-293T (ATCC; VA, USA; CRL-11268) cells were cultured in complete Iscove's Modified Dulbecco's Medium (IMDM) (Sigma-Aldrich; distributed by Merck Life Science UK Ltd., Watford, UK; I3390) supplemented with 10% fetal bovine serum (Sigma-Aldrich; distributed by Merck Life Science UK Ltd., Watford, UK; F7524) and 2 mM GlutaMAX-1 (Gibco; distributed by ThermoFisher Scientific, Loughborough, UK; 35050) in a 175-cm^2 tissue culture-treated flask in a humidified incubator at 37°C and 5% CO_2 atmosphere.

Plasmids

The *Anabaena* PIE self-splicing RNA sequence[46] and BE4max coding sequence (taken from AddGene plasmid 112093) were cloned by Golden Gate assembly using ∼1 kb gBlock fragments (Integrated DNA Technologies (IDT); Leuven, Belgium). Fragments were amplified by PCR using Q5 High-Fidelity DNA polymerase (New England

Biolabs [NEB], Hitchin, UK; M0491), dNTPs (NEB; N0447L) and custom oligonucleotides (IDT), agarose gel purified using the QIAquick gel extraction kit (Qiagen; Manchester, UK; 28706) and ligated into a pUC-derived plasmid (Blue Heron Biotech; WA, USA) using T4 DNA ligase (Roche; distributed by Merck Life Science UK Ltd., Watford, UK; 10716359001). High-efficiency chemically competent bacteria (5-alpha competent *E. coli*; NEB; C2987) were transformed with the ligation reactions, plated onto antibiotic-laden LB agar plates, and incubated overnight at 37°C.

In vitro transcription

The plasmid DNA template for circRNA production was linearized by digestion with a restriction endonuclease whose site was 3′ to the transcript, while the DNA template for linear mRNA production was amplified from plasmid DNA, using a reverse primer that incorporated a 120-base poly(A) tail. RNA was synthesized from linear DNA templates using the HiScribe T7 Quick High Yield RNA Synthesis Kit (NEB; E2050S), according to the manufacturer's instructions. After synthesis, RNA was precipitated using LiCl supplied with the HiScribe T7 Quick High Yield RNA Synthesis Kit. Linear RNA was 7-methylguanylate capped using the Vaccinia Capping System (NEB; M2080S) and methylated using 2′-O-methyltransferase (NEB; M0366S) according to the manufacturer's instructions. CircRNA does not require capping or methylation and was resuspended in a circularization buffer containing 50 mM Tris-HCl, pH 7.5 (Invitrogen; distributed by ThermoFisher Scientific, Loughborough, UK; 15567-027), 10 mM $MgCl_2$ (Invitrogen; AM9530G), 1 mM dithiothreitol (ThermoFisher Scientific; 707265ML), and 2 mM guanosine triphosphate (ThermoFisher Scientific; R1461) and was heated to 55°C for 15 min to allow back-splicing to occur. Capped and methylated mRNA or circRNA was purified by LiCl precipitation, resuspended in TE buffer, pH 7.5 (IDT; 11-01-02-02) and quantified using the Qubit RNA Broad Range (BR) Assay Kit (Invitrogen; Q10211). Purified RNA was checked for size and integrity using the 2200 TapeStation and RNA ScreenTape reagents (Agilent; Cheshire, UK; RNA ScreenTape; 5067–5576, Sample Buffer; 5067–5577, Ladder; 5067–5578).

Production of lentiviral supernatant

HEK-293T cells were plated in 10-cm tissue culture-treated plates and were transfected at >70% confluency with a VSV-G envelope expression plasmid, an REV expression plasmid, a Gag-Pol expression plasmid, and the transgene of interest expressed in a lentiviral (pCCL) vector plasmid at a ratio of 1:1:2:4 (total DNA = 12.5 μg). Transfections were conducted with GeneJuice (Millipore; distributed by Merck Life Science UK Ltd., Watford, UK; 70967) according to the manufacturer's instructions and viral supernatants were harvested at 48 h post-transfection. Supernatants were pelleted at 400 x *g* for 5 min to remove cellular debris and were filtered through a 0.45-μM filter before storing at −80°C.

Titration of viral supernatants

Functional viral titers were calculated using thawed lentiviral supernatant on HEK-293T cells. Lentiviral supernatant was serially diluted and added to HEK-293T cells plated at 50,000 cells per well of a tissue culture-treated 24-well plate in complete IMDM containing 8 μg/mL polybrene (Millipore; TR-1003-G). Transduction was performed by centrifugation at 1,000 x *g* for 10 min before transfer to a 37°C incubator with 5% CO_2. The percentage of transduced cells was identified by flow cytometry 72 h later, using the anti-CAT-19 idiotype antibody (Autolus; London, UK; produced in-house). Functional viral titers were calculated, using the equation below, from the cells transduced with <20% efficiency, to aim for a vector copy number of one integration per cell.

$$\begin{aligned} \textit{Viral titer}\ (\textit{Transducing units}\ (TU)\ /\ mL)\ =\ (\textit{number of} \\ \textit{cells plated}\ x\ (\%\ \textit{transduction efficiency}\ /\ 100))\ / \\ (\textit{vector volume}\ \text{in}\ mL) \end{aligned}$$

Primary cell culture

PBMCs were isolated from whole human blood (NHS Blood and Transplant; London, UK) by density gradient centrifugation using Ficoll-Paque PLUS (Sigma-Aldrich; 17-1440-02) and SepMate-50 Tubes (STEMCELL Technologies, Cambridge, UK; 85450). Isolated PBMCs were cryopreserved prior to use and were thawed and cultured in TexMACS GMP Medium (Miltenyi Biotec; Woking, UK; 170-076-306) containing 3% human serum AB off-the-clot (BioIVT; West Sussex, UK; HUMANABSRMC-1) and 10 ng/mL interleukin-7 and -15 (Miltenyi Biotec; IL-7; 130-095-367, IL-15; 130-095-760). Isolated PBMCs were activated using a 1:100 ratio of TransAct (Miltenyi Biotec; 130-111-160) to T cells in cell culture flasks for a duration of 48 h prior to base editing.

For large-scale experiments, T cells were separated from leukapheresis material using anti-CD4 and anti-CD8 magnetic microbeads (Miltenyi Biotec; CD4; 276-01, CD8; 275-01) on the CliniMACS Prodigy instrument (Miltenyi Biotec). The tubing sets (Miltenyi Biotec; 170-076-600) were installed on the Prodigy and positive selection of the $CD4^+$- and $CD8^+$-labeled T cells was carried out according to standard protocols. Sorted T cells were activated using GMP-grade TransAct (Miltenyi Biotec; 170-076-156) according to the manufacturer's protocol and were cultured in a 100M G-Rex (Wilson Wolf; MN, USA; RU81100).

Base editing

RNAs were delivered to stimulated PBMCs or $CD4^+$/$CD8^+$sorted T cells using either the 4D or large volume (LV) Nucleofector and corresponding kits (Lonza, Basel, Switzerland; P3 Primary Cell 4D-Nucleofector X Kit L; V4XP-3024, LV Kit L; V4LP-3002) and pulse code EH-115 on day 2 of the process. Cells were harvested from the culture vessel, pelleted by centrifugation at 400 × *g* for 5 min at ambient temperature, and resuspended in 1 volume of Dulbecco's phosphate-buffered saline (PBS) (Sigma-Aldrich; D8537-500ML). This washing procedure was repeated one more time, re-suspending the cells in 0.5 volume of PBS, before pelleting the cells and re-suspending in P3 electroporation buffer at a density of 5×10^7 cells/mL. T cells were electroporated with a fixed amount of sgRNA (Genscript)

(30 pmol/1 × 10^6 cells) and varying amounts of linear or circular RNA encoding the base editor enzyme. Base editor RNA was added from a concentrated stock (1 mg/mL) to the P3 electroporation buffer to achieve the desired concentration (ranging from 0.25–4.00 μg RNA/ 1 × 10^6 cells).

Immediately after electroporation, T cells were diluted 1:5 with cytokine-free medium and were placed in an incubator at 37°C and 5% CO_2 and cells were left to recover for 10–15 min. Transfected T cells were then transferred to the appropriate culture vessels at a concentration of 1 to 2 × 10^6 cells/mL. For small-scale experiments, base-edited T cells were cultured in 24-well plates and were placed in a humidified 37°C incubator for 4 days; at which point, half of the T cell culture was restimulated with TransAct to up-regulate the expression of the T cell inhibitory receptors, to allow the identification of gene knockouts by flow cytometry. For large-scale experiments, base-edited T cells were cultured in a six-well G-Rex (Wilson Wolf; 80240M) and were placed in a humidified 37°C incubator and left to recover overnight, before transduction to introduce the CAR genes.

Lentiviral transduction of anti-CD19 CAR T cells

Sorted T cells were transduced with lentiviral supernatant encoding an anti-CD19 CAR[49–52] on day 3 of the process (24 h post-nucleofection) using a multiplicity of infection of 5. T cells were seeded at a cell density of 1 × 10^6 cells/mL with lentiviral supernatant in RetroNectin-coated (Takara, London, UK; T100A) 100-mL differentiation bags (Miltenyi Biotec; 170-076-400) and were placed in an incubator at 37°C and 5% CO_2. Expression of the transgene was assessed on day 7 of the process by flow cytometry using an anti-idiotype antibody to detect the anti-CD19 scFv (Autolus; produced in-house).

Flow cytometry and antibodies

Flow cytometry was performed using the MACSQuant10 or X instruments (Miltenyi Biotec). Unless otherwise stated, antibodies were prepared at dilutions recommended by the manufacturer in PBS (Sigma-Aldrich; D8537-500ML) and all staining was performed at ambient temperature for 10 min, protected from light. Samples were resuspended in 50–100 μL PBS or viability stain and 80% of the volume was analyzed by flow cytometry. Cell viability dyes used were Zombie-NIR (BioLegend; London, UK; 423106) or SYTOX AAdvanced (ThermoFisher Scientific; S10274). Isotype and/or non-transduced samples were included as negative controls for flow cytometry gating.

Antibodies were sourced from BioLegend, unless otherwise stated. Antibodies used in small-scale experiments were: CD3-PE-Cy7 (344816), CD279 (PD-1)-PE (329906), CD366 (TIM3)-BV421 (345008), IgG1 isotype control PE (400112), and IgG1 isotype control BV421 (400158). For large-scale experiments, the antibodies were sourced from Miltenyi Biotec, unless otherwise indicated, and consisted of: CD3-VioGreen (130-113-142), CD8-VioBlue (130-110-683), CD279 (PD-1)-PE (130-120-382), CD366 (TIM3)-PE-Vio770 (130-121-334), CD223 (LAG3)-VioBright515 (130-120-012), CCR7-PE (130-119-583), CD45RA-APC-Vio770 (130-117-747), REA control PE (130-113-438), REA control VioBright515 (130-113-445), REA control PE-Vio770 (130-113-440), and REA control APC-Vio770 (130-113-435). Expression of the CAR was detected using an anti-CAT-19 scFv Rat Fc idiotype antibody (Autolus; produced in-house) and an APC-conjugated anti-Rat Fc secondary antibody (BioLegend; 405407).

Flow cytometry data were analyzed using FlowJo Software, version 10.8.1. The gating strategy first involved the identification of the cell population based on size and granularity (FSC-A versus SSC-A), before isolating the singlets (FSC-A versus FSC-H) and live cells (negative for viability dye). T cells were identified as $CD3^+$ prior to subsequent gating on the markers of interest.

Genotyping

Genomic DNA was isolated from 1 × 10^6 T cells on day 9 of the process using the PureLink Genomic DNA Mini Kit (Invitrogen; K182002). An 800-base pair region spanning the target site was amplified by nested PCR, and the amplicon was purified using the QIAquick PCR Purification Kit (Qiagen; 28106) and sent for Sanger sequencing (Source BioScience). Sanger sequencing traces were uploaded to EditR (http://baseeditr.com/),[48] and the frequency of base conversion was determined for each base within the protospacer sequence.

RNA isolation

RNA was isolated from 1 × 10^6 T cells using the Quick-DNA/RNA Microprep Plus Kit (Zymo Research; distributed from Cambridge Bioscience, Cambridge, UK; D7005T), according to the manufacturer's instructions. DNA was digested in the RNA column using 5 U of DNase I (Zymo Research; D7005T) for 15 min at ambient temperature. RNA was eluted in 15 mL of elution buffer and concentrations determined on the Qubit 4 Fluorometer (Invitrogen, ThermoFisher Scientific) using the Qubit RNA BR assay kit (Invitrogen; Q10211).

RT-qPCR

Primers and probes for qPCR and RT-qPCR were designed using PrimerQuest (IDT) and custom synthesized (IDT). The sequences of the primers and probe were: BE4max forward, 5′-CCCAAGAG GAACAGCGATAAG-3′; BE4max reverse, 5′-CCACCACCAGCAC AGAATAG-3′; BE4max probe, 5′-/56-FAM/ATCGCCAGA/ZEN/ AAGAAGGACTGGGAC/3IABkFQ/-3′; GAPDH forward, 5′-ACAT CGCTCAGACACCATG-3′; GAPDH reverse 5′- TGTAGTTGAGG TCAATGAAGGG-3′; and GAPDH probe 5′-/5HEX/AAGGTCG GA/ZEN/GTCAACGGATTTGGTC/3IABkFQ/-3′. DNA and RNA were extracted from T cells using Quick-DNA/RNA Microprep Plus kit (Zymo Research; D7005T) according to the manufacturer's instructions. Purified RNA was quantified using Qubit RNA Broad Range (BR) Assay Kit (Invitrogen; Q10211), and samples diluted to 25 ng/mL with TE buffer (Synthego) in preparation for RT-qPCR analysis. Each 20-μL reaction contained 300 nM forward and reverse primer, 250 nM probe, and 1x PrimeTime One-step RT-qPCR Master Mix (IDT; 10007066). A master mix was prepared in a dedicated class II biosafety cabinet and distributed into the wells of a hard-shell,

thin-walled 96-well PCR plate (Bio-Rad; Watford, UK; HSP9665). Sample templates and standards were added to the 96-well PCR plate, prior to sealing with Microseal B adhesive sealer (Bio-Rad; MSB-1001) and cycling on a Bio-Rad CFX96 Real-Time System qPCR machine (Bio-Rad) running on CFX Maestro 1.1 (version 4.1.2433.1219) software (Bio-Rad). Transcript copy number was determined using CFX Maestro 1.1 software, and where appropriate, normalization to GAPDH copy number was carried out to account for variation in the amount of RNA template used.

Western blotting

Cell pellets (1×10^6 T cells) were obtained at 24, 48, 72, and 96 h post-nucleofection with BE4max-encoding linear or circular RNA (4.00 μg RNA/1×10^6 cells) and a non-targeting sgRNA. Samples were lysed in RIPA Lysis Buffer (Millipore; 20–188) supplemented with Protease Inhibitor Cocktail Set III (Millipore; 539134), according to the manufacturer's protocol. Where appropriate, the amount of protein was quantified using the Pierce BCA Protein Assay Kit (ThermoScientific; 23227) and 15 μg of protein was denatured in NuPAGE LDS Sample Buffer (Invitrogen; NP0007) supplemented with β-mercaptoethanol (Bio-Rad; 1610710) at a final concentration of 2.5%, by boiling the samples at 95°C for 5 min. Samples were run on a 7.5% Mini-PROTEAN Precast TGX Protein Gel (Bio-Rad; 4561024) according to the manufacturer's instructions. The proteins were transferred to a Trans-Blot Turbo Midi 0.2 μm Nitrocellulose Transfer Pack (Bio-Rad; 1704159), using the Trans-Blot Turbo Transfer System (Bio-Rad) and a pre-defined protocol for high molecular weight proteins (transfer time; 10 min). The membrane was blocked with 5% milk in PBS, 0.1% TWEEN 20 (Sigma-Aldrich; P2287-500ML) for 1 h at ambient temperature, prior to blotting overnight at 4°C with either a mouse anti-β-actin antibody (Sigma-Aldrich; A5316; at a 1:10,000 dilution) or a mouse anti-Cas9 antibody mix (anti-Cas9 [clone 7A9-3A8]; Cell Signaling Technologies, MA, USA; 14697S and anti-CRISPR [Cas9] (clone 7A9); BioLegend; 844301, with or without the addition of anti-CRISPR [Cas9] (clone 6G12-H11); BioLegend; 698302, all antibodies were prepared at a 1:1,000 dilution). Following washing in PBS 0.1% TWEEN 20, the membrane was blotted with a secondary HRP-linked goat anti-mouse antibody (BioLegend; 405306) at a 1:5,000 dilution for 1 h at ambient temperature. All antibody mixes were prepared in 2.5% milk PBS 0.1% TWEEN 20. Protein was visualized using the Pierce ECL Western Blotting Substrate (ThermoFisher Scientific; 32106).

Statistical analysis

Two-way analysis of variance (ANOVA) was used for the comparison of multiple datasets. Data are represented as mean with error bars, where appropriate, to indicate the standard deviation. GraphPad Prism software (version 9.3.0) was used to calculate statistical analyses, using a p value <0.05 to indicate statistical significance.

Ethical considerations

Peripheral blood was obtained from healthy human donors after informed and written consent, in accordance with the regulations of the Human Tissue Authority (United Kingdom).

DATA AND CODE AVAILABILITY

Source data are available from the corresponding author upon request.

SUPPLEMENTAL INFORMATION

Supplemental information can be found online at https://doi.org/10.1016/j.omtm.2023.101123.

ACKNOWLEDGMENTS

M.P. is supported by the UK National Health Service Biomedical Research Centre at University College London Hospitals. The authors would like to acknowledge Mike Merges for his support of the project. The diagrammatic figures in this study were created with BioRender.com.

AUTHOR CONTRIBUTIONS

Conceptualization: R.W., G.S.T., K.L., C.R., J.S., and M.P. Methodology, investigation, and visualization: R.W., F.P., K.L., C.A., K.S., J.H., A.W., G.S.T., and J.S. Supervision: R.W., G.S.T, K.L., J.S., and M.P. Writing: R.W., K.L., J.S., and M.P. Manuscript review: all authors.

DECLARATION OF INTERESTS

R.W., F.P., K.L., L.M., C.A., A.W., G.S.T, K.L., J.S., and M.P. are employees of Autolus Therapeutics plc and hold equity shares or options in the company. M.P. receives royalty share from patents licensed to Autolus Therapeutics plc.

REFERENCES

1. Stadtmauer, E.A., Fraietta, J.A., Davis, M.M., Cohen, A.D., Weber, K.L., Lancaster, E., Mangan, P.A., Kulikovskaya, I., Gupta, M., Chen, F., et al. (2020). CRISPR-engineered T cells in patients with refractory cancer. Science *367*, eaba7365. https://doi.org/10.1126/science.aba7365.

2. Rupp, L.J., Schumann, K., Roybal, K.T., Gate, R.E., Ye, C.J., Lim, W.A., and Marson, A. (2017). CRISPR/Cas9-mediated PD-1 disruption enhances anti-tumor efficacy of human chimeric antigen receptor T cells. Sci. Rep. *7*, 737. https://doi.org/10.1038/s41598-017-00462-8.

3. Alishah, K., Birtel, M., Masoumi, E., Jafarzadeh, L., Mirzaee, H.R., Hadjati, J., Voss, R.-H., Diken, M., and Asad, S. (2021). CRISPR/Cas9-mediated TGFβRII disruption enhances anti-tumor efficacy of human chimeric antigen receptor T cells in vitro. J. Transl. Med. *19*, 482. https://doi.org/10.1186/s12967-021-03146-0.

4. Tang, N., Cheng, C., Zhang, X., Qiao, M., Li, N., Mu, W., Wei, X.-F., Han, W., and Wang, H. (2020). TGF-β inhibition via CRISPR promotes the long-term efficacy of CAR T cells against solid tumors. JCI Insight *5*, e133977. https://doi.org/10.1172/jci.insight.133977.

5. Qasim, W., Ciocarlie, O., Adams, S., Inglott, S., Murphy, C., Rivat, C., Wright, G., Lucchini, G., Silva, J., Rao, K., et al. (2017). Preliminary Results of UCART19, an Allogeneic Anti-CD19 CAR T-Cell Product in a First-in-Human Trial (PALL) in Pediatric Patients with CD19+ Relapsed/Refractory B-Cell Acute Lymphoblastic Leukemia. Blood *130*, 1271.

6. Eyquem, J., Mansilla-Soto, J., Giavridis, T., van der Stegen, S.J.C., Hamieh, M., Cunanan, K.M., Odak, A., Gönen, M., and Sadelain, M. (2017). Targeting a CAR to the TRAC locus with CRISPR/Cas9 enhances tumour rejection. Nature *543*, 113–117. https://doi.org/10.1038/nature21405.

7. Roth, T.L., Puig-Saus, C., Yu, R., Shifrut, E., Carnevale, J., Li, P.J., Hiatt, J., Saco, J., Krystofinski, P., Li, H., et al. (2018). Reprogramming human T cell function and specificity with non-viral genome targeting. Nature *559*, 405–409. https://doi.org/10.1038/s41586-018-0326-5.

8. MacLeod, D.T., Antony, J., Martin, A.J., Moser, R.J., Hekele, A., Wetzel, K.J., Brown, A.E., Triggiano, M.A., Hux, J.A., Pham, C.D., et al. (2017). Integration of a CD19 CAR into the TCR Alpha Chain Locus Streamlines Production of Allogeneic Gene-Edited CAR T Cells. Mol. Ther. *25*, 949–961. https://doi.org/10.1016/j.ymthe.2017.02.005.

9. Roth, T.L., Li, P.J., Blaeschke, F., Nies, J.F., Apathy, R., Mowery, C., Yu, R., Nguyen, M.L.T., Lee, Y., Truong, A., et al. (2020). Pooled Knockin Targeting for Genome Engineering of Cellular Immunotherapies. Cell *181*, 728–744.e21. https://doi.org/10.1016/j.cell.2020.03.039.

10. Odak, A., Yuan, H., Feucht, J., Mansilla - Soto, J., Eyquem, J., Leslie, C., and Sadelain, M. (2020). Targeted Integration of a CAR at a Novel Genomic Safe Harbor Directs Potent Therapeutic Outcomes. Blood *136*, 28. https://doi.org/10.1182/blood-2020-141967.

11. Lombardo, A., Cesana, D., Genovese, P., Di Stefano, B., Provasi, E., Colombo, D.F., Neri, M., Magnani, Z., Cantore, A., Lo Riso, P., et al. (2011). Site-specific integration and tailoring of cassette design for sustainable gene transfer. Nat. Methods *8*, 861–869. https://doi.org/10.1038/nmeth.1674.

12. Leibowitz, M.L., Papathanasiou, S., Doerfler, P.A., Blaine, L.J., Sun, L., Yao, Y., Zhang, C.-Z., Weiss, M.J., and Pellman, D. (2021). Chromothripsis as an on-target consequence of CRISPR–Cas9 genome editing. Nat. Genet. *53*, 895–905. https://doi.org/10.1038/s41588-021-00838-7.

13. Nahmad, A.D., Reuveni, E., Goldschmidt, E., Tenne, T., Liberman, M., Horovitz-Fried, M., Khosravi, R., Kobo, H., Reinstein, E., Madi, A., et al. (2022). Frequent aneuploidy in primary human T cells after CRISPR–Cas9 cleavage. Nat. Biotechnol. *40*, 1807–1813. https://doi.org/10.1038/s41587-022-01377-0.

14. Poirot, L., Philip, B., Schiffer-Mannioui, C., Le Clerre, D., Chion-Sotinel, I., Derniame, S., Potrel, P., Bas, C., Lemaire, L., Galetto, R., et al. (2015). Multiplex Genome-Edited T-cell Manufacturing Platform for "Off-the-Shelf" Adoptive T-cell Immunotherapies. Cancer Res. *75*, 3853–3864. https://doi.org/10.1158/0008-5472.CAN-14-3321.

15. Qasim, W., Zhan, H., Samarasinghe, S., Adams, S., Amrolia, P., Stafford, S., Butler, K., Rivat, C., Wright, G., Somana, K., et al. (2017). Molecular remission of infant B-ALL after infusion of universal TALEN gene-edited CAR T cells. Sci. Transl. Med. *9*, eaaj2013. https://doi.org/10.1126/scitranslmed.aaj2013.

16. Glaser, V., Flugel, C., Kath, J., Du, W., Drosdek, V., Franke, C., Stein, M., Pruß, A., Schmueck-Henneresse, M., Volk, H.-D., et al. (2023). Combining different CRISPR nucleases for simultaneous knock-in and base editing prevents translocations in multiplex-edited CAR T cells. Genome Biol. *24*, 89. https://doi.org/10.1186/s13059-023-02928-7.

17. Georgiadis, C., Rasaiyaah, J., Gkazi, S.A., Preece, R., Etuk, A., Christi, A., and Qasim, W. (2021). Base-edited CAR T cells for combinational therapy against T cell malignancies. Leukemia *35*, 3466–3481. https://doi.org/10.1038/s41375-021-01282-6.

18. Webber, B.R., Lonetree, C.L., Kluesner, M.G., Johnson, M.J., Pomeroy, E.J., Diers, M.D., Lahr, W.S., Draper, G.M., Slipek, N.J., Smeester, B.A., et al. (2019). Highly efficient multiplex human T cell engineering without double-strand breaks using Cas9 base editors. Nat. Commun. *10*, 5222. https://doi.org/10.1038/s41467-019-13007-6.

19. Kuscu, C., Parlak, M., Tufan, T., Yang, J., Szlachta, K., Wei, X., Mammadov, R., and Adli, M. (2017). CRISPR-STOP: gene silencing through base-editing-induced nonsense mutations. Nat. Methods *14*, 710–712. https://doi.org/10.1038/nmeth.4327.

20. Gapinske, M., Luu, A., Winter, J., Woods, W.S., Kostan, K.A., Shiva, N., Song, J.S., and Perez-Pinera, P. (2018). CRISPR-SKIP: programmable gene splicing with single base editors. Genome Biol. *19*, 107. https://doi.org/10.1186/s13059-018-1482-5.

21. Billon, P., Bryant, E.E., Joseph, S.A., Nambiar, T.S., Hayward, S.B., Rothstein, R., and Ciccia, A. (2017). CRISPR-Mediated Base Editing Enables Efficient Disruption of Eukaryotic Genes through Induction of STOP Codons. Mol. Cell *67*, 1068–1079.e4. https://doi.org/10.1016/j.molcel.2017.08.008.

22. Koblan, L.W., Erdos, M.R., Wilson, C., Cabral, W.A., Levy, J.M., Xiong, Z.-M., Tavarez, U.L., Davison, L.M., Gete, Y.G., Mao, X., et al. (2021). In vivo base editing rescues Hutchinson–Gilford progeria syndrome in mice. Nature *589*, 608–614. https://doi.org/10.1038/s41586-020-03086-7.

23. Whisenant, D., Lim, K., Revêchon, G., Yao, H., Bergo, M.O., Machtel, P., Kim, J.-S., and Eriksson, M. (2022). Transient expression of an adenine base editor corrects the Hutchinson-Gilford progeria syndrome mutation and improves the skin phenotype in mice. Nat. Commun. *13*, 3068. https://doi.org/10.1038/s41467-022-30800-y.

24. Newby, G.A., Yen, J.S., Woodard, K.J., Mayuranathan, T., Lazzarotto, C.R., Li, Y., Sheppard-Tillman, H., Porter, S.N., Yao, Y., Mayberry, K., et al. (2021). Base editing of haematopoietic stem cells rescues sickle cell disease in mice. Nature *595*, 295–302. https://doi.org/10.1038/s41586-021-03609-w.

25. Gaudelli, N.M., Komor, A.C., Rees, H.A., Packer, M.S., Badran, A.H., Bryson, D.I., and Liu, D.R. (2017). Programmable base editing of A•T to G•C in genomic DNA without DNA cleavage. Nature *551*, 464–471. https://doi.org/10.1038/nature24644.

26. Gaudelli, N.M., Lam, D.K., Rees, H.A., Solá-Esteves, N.M., Barrera, L.A., Born, D.A., Edwards, A., Gehrke, J.M., Lee, S.-J., Liquori, A.J., et al. (2020). Directed evolution of adenine base editors with increased activity and therapeutic application. Nat. Biotechnol. *38*, 892–900. https://doi.org/10.1038/s41587-020-0491-6.

27. Komor, A.C., Kim, Y.B., Packer, M.S., Zuris, J.A., and Liu, D.R. (2016). Programmable editing of a target base in genomic DNA without double-stranded DNA cleavage. Nature *533*, 420–424. https://doi.org/10.1038/nature17946.

28. Chen, L., Zhu, B., Ru, G., Meng, H., Yan, Y., Hong, M., Zhang, D., Luan, C., Zhang, S., Wu, H., et al. (2023). Re-engineering the adenine deaminase TadA-8e for efficient and specific CRISPR-based cytosine base editing. Nat. Biotechnol. *41*, 663–672. https://doi.org/10.1038/s41587-022-01532-7.

29. Neugebauer, M.E., Hsu, A., Arbab, M., Krasnow, N.A., McElroy, A.N., Pandey, S., Doman, J.L., Huang, T.P., Raguram, A., Banskota, S., et al. (2023). Evolution of an adenine base editor into a small, efficient cytosine base editor with low off-target activity. Nat. Biotechnol. *41*, 673–685. https://doi.org/10.1038/s41587-022-01533-6.

30. Lam, D.K., Feliciano, P.R., Arif, A., Bohnuud, T., Fernandez, T.P., Gehrke, J.M., Grayson, P., Lee, K.D., Ortega, M.A., Sawyer, C., et al. (2023). Improved cytosine base editors generated from TadA variants. Nat. Biotechnol. *41*, 686–697. https://doi.org/10.1038/s41587-022-01611-9.

31. Zeng, J., Wu, Y., Ren, C., Bonanno, J., Shen, A.H., Shea, D., Gehrke, J.M., Clement, K., Luk, K., Yao, Q., et al. (2020). Therapeutic base editing of human hematopoietic stem cells. Nat. Med. *26*, 535–541. https://doi.org/10.1038/s41591-020-0790-y.

32. Arbab, M., Matuszek, Z., Kray, K.M., Du, A., Newby, G.A., Blatnik, A.J., Raguram, A., Richter, M.F., Zhao, K.T., Levy, J.M., et al. (2023). Base editing rescue of spinal muscular atrophy in cells and in mice. Science *380*, eadg6518. https://doi.org/10.1126/science.adg6518.

33. Lee, R.G., Mazzola, A.M., Braun, M.C., Platt, C., Vafai, S.B., Kathiresan, S., Rohde, E., Bellinger, A.M., and Khera, A.V. (2023). Efficacy and Safety of an Investigational Single-Course CRISPR Base-Editing Therapy Targeting PCSK9 in Nonhuman Primate and Mouse Models. Circulation *147*, 242–253. https://doi.org/10.1161/CIRCULATIONAHA.122.062132.

34. Rothgangl, T., Dennis, M.K., Lin, P.J.C., Oka, R., Witzigmann, D., Villiger, L., Qi, W., Hruzova, M., Kissling, L., Lenggenhager, D., et al. (2021). In vivo adenine base editing of PCSK9 in macaques reduces LDL cholesterol levels. Nat. Biotechnol. *39*, 949–957. https://doi.org/10.1038/s41587-021-00933-4.

35. Diorio, C., Murray, R., Naniong, M., Barrera, L., Camblin, A., Chukinas, J., Coholan, L., Edwards, A., Fuller, T., Gonzales, C., et al. (2022). Cytosine base editing enables quadruple-edited allogeneic CART cells for T-ALL. Blood *140*, 619–629. https://doi.org/10.1182/blood.2022015825.

36. Chiesa, R., Georgiadis, C., Syed, F., Zhan, H., Etuk, A., Gkazi, S.A., Preece, R., Ottaviano, G., Braybrook, T., Chu, J., et al. (2023). Base-Edited CAR7 T Cells for Relapsed T-Cell Acute Lymphoblastic Leukemia. N. Engl. J. Med. *389*, 899–910. https://doi.org/10.1056/NEJMoa2300709.

37. Jang, H.-K., Jo, D.H., Lee, S.-N., Cho, C.S., Jeong, Y.K., Jung, Y., Yu, J., Kim, J.H., Woo, J.-S., and Bae, S. (2021). High-purity production and precise editing of DNA base editing ribonucleoproteins. Sci. Adv. *7*, 2661. https://doi.org/10.1126/sciadv.abg2661.

38. Schlee, M., and Hartmann, G. (2016). Discriminating self from non-self in nucleic acid sensing. Nat. Rev. Immunol. *16*, 566–580. https://doi.org/10.1038/nri.2016.78.

39. Hornung, V., Ellegast, J., Kim, S., Brzózka, K., Jung, A., Kato, H., Poeck, H., Akira, S., Conzelmann, K.-K., Schlee, M., et al. (2006). 5'-Triphosphate RNA Is the Ligand for RIG-I. Science *314*, 994–997. https://doi.org/10.1126/science.1132505.

40. England, T.E., and Uhlenbeck, O.C. (1978). Enzymatic oligoribonucleotide synthesis with T4 RNA ligase. Biochemistry *17*, 2069–2076. https://doi.org/10.1021/bi00604a008.

41. Chen, C.Y., and Sarnow, P. (1995). Initiation of protein synthesis by the eukaryotic translational apparatus on circular RNAs. Science *268*, 415–417. https://doi.org/10.1126/science.7536344.

42. Petkovic, S., and Müller, S. (2015). RNA circularization strategies in vivo and in vitro. Nucleic Acids Res. *43*, 2454–2465. https://doi.org/10.1093/nar/gkv045.

43. Michel, F., and Westhof, E. (1990). Modelling of the Three-dimensional Architecture of Group I Catalytic Introns Based on Comparative Sequence Analysis. J. Mol. Biol. *216*, 585–610.

44. Price, J.V., Engberg, J., and Cech, T.R. (1987). 5' exon requirement for self-splicing of the Tetrahymena thermophila pre-ribosomal RNA and identification of a cryptic 5' splice site in the 3' exon. J. Mol. Biol. *196*, 49–60. https://doi.org/10.1016/0022-2836(87)90510-9.

45. Puttaraju, M., and Been, M.D. (1992). Group I permuted intron-exon (PIE) sequences self-splice to produce circular exons. Nucleic Acids Res. *20*, 5357–5364. https://doi.org/10.1093/nar/20.20.5357.

46. Wesselhoeft, R.A., Kowalski, P.S., and Anderson, D.G. (2018). Engineering circular RNA for potent and stable translation in eukaryotic cells. Nat. Commun. *9*, 2629. https://doi.org/10.1038/s41467-018-05096-6.

47. Chen, R., Wang, S.K., Belk, J.A., Amaya, L., Li, Z., Cardenas, A., Abe, B.T., Chen, C.-K., Wender, P.A., and Chang, H.Y. (2023). Engineering circular RNA for enhanced protein production. Nat. Biotechnol. *41*, 262–272. https://doi.org/10.1038/s41587-022-01393-0.

48. Kluesner, M.G., Nedveck, D.A., Lahr, W.S., Garbe, J.R., Abrahante, J.E., Webber, B.R., and Moriarity, B.S. (2018). EditR: A Method to Quantify Base Editing from Sanger Sequencing. CRISPR J. *1*, 239–250. https://doi.org/10.1089/crispr.2018.0014.

49. Ghorashian, S., Kramer, A.M., Onuoha, S., Wright, G., Bartram, J., Richardson, R., Albon, S.J., Casanovas-Company, J., Castro, F., Popova, B., et al. (2019). Enhanced CAR T cell expansion and prolonged persistence in pediatric patients with ALL treated with a low-affinity CD19 CAR. Nat. Med. *25*, 1408–1414. https://doi.org/10.1038/s41591-019-0549-5.

50. Ghorashian, S., Kramer, A.M., Albon, S.J., Wright, G., Castro, F., Popova, B., Casanovas Company, J., Irving, C., Vetharoy, W., Richardson, R., et al. (2017). A Novel Low Affinity CD19CAR Results in Durable Disease Remissions and Prolonged CAR T Cell Persistence without Severe CRS or Neurotoxicity in Patients with Paediatric ALL. Blood *130*, 806.

51. Ghorashian, S., Kramer, A.M., Albon, S.J., Irving, C., Chan, L., Castro, F., Popova, B., Champion, K., Wright, G., Zhan, H., et al. (2016). A Novel Second Generation CD19 CAR for Therapy of High Risk/Relapsed Paediatric CD19+ Acute Lymphoblastic Leukaemia and Other Haematological Malignancies: Preliminary Results from the Carpall Study. Blood *128*, 4026.

52. Roddie, C., Dias, J., O'Reilly, M.A., Abbasian, M., Cadinanos-Garai, A., Vispute, K., Bosshard-Carter, L., Mitsikakou, M., Mehra, V., Roddy, H., et al. (2021). Durable Responses and Low Toxicity After Fast Off-Rate CD19 Chimeric Antigen Receptor-T Therapy in Adults With Relapsed or Refractory B-Cell Acute Lymphoblastic Leukemia. J. Clin. Oncol. *39*, 3352–3363. https://doi.org/10.1200/JCO.21.00917.

53. Hadas, Y., Sultana, N., Youssef, E., Sharkar, M.T.K., Kaur, K., Chepurko, E., and Zangi, L. (2019). Optimizing Modified mRNA In Vitro Synthesis Protocol for Heart Gene Therapy. Mol. Ther. Methods Clin. Dev. *14*, 300–305. https://doi.org/10.1016/j.omtm.2019.07.006.

54. Vaidyanathan, S., Azizian, K.T., Haque, A.K.M.A., Henderson, J.M., Hendel, A., Shore, S., Antony, J.S., Hogrefe, R.I., Kormann, M.S.D., Porteus, M.H., and McCaffrey, A.P. (2018). Uridine Depletion and Chemical Modification Increase Cas9 mRNA Activity and Reduce Immunogenicity without HPLC Purification. Mol. Ther. Nucleic Acids *12*, 530–542. https://doi.org/10.1016/j.omtn.2018.06.010.

55. Gallie, D.R. (1998). A tale of two termini: A functional interaction between the termini of an mRNA is a prerequisite for efficient translation initiation. Gene *216*, 1–11. https://doi.org/10.1016/S0378-1119(98)00318-7.

56. Kruger, K., Grabowski, P.J., Zaug, A.J., Sands, J., Gottschling, D.E., and Cech, T.R. (1982). Self-splicing RNA: autoexcision and autocyclization of the ribosomal RNA intervening sequence of Tetrahymena. Cell *31*, 147–157. https://doi.org/10.1016/0092-8674(82)90414-7.

57. Ford, E., and Ares, M. (1994). Synthesis of circular RNA in bacteria and yeast using RNA cyclase ribozymes derived from a group I intron of phage T4. Proc. Natl. Acad. Sci. USA *91*, 3117–3121. https://doi.org/10.1073/pnas.91.8.3117.

58. Litke, J.L., and Jaffrey, S.R. (2019). Highly efficient expression of circular RNA aptamers in cells using autocatalytic transcripts. Nat. Biotechnol. *37*, 667–675. https://doi.org/10.1038/s41587-019-0090-6.

59. Filonov, G.S., Moon, J.D., Svensen, N., and Jaffrey, S.R. (2014). Broccoli: Rapid Selection of an RNA Mimic of Green Fluorescent Protein by Fluorescence-Based Selection and Directed Evolution. J. Am. Chem. Soc. *136*, 16299–16308. https://doi.org/10.1021/ja508478x.

60. Jost, I., Shalamova, L.A., Gerresheim, G.K., Niepmann, M., Bindereif, A., and Rossbach, O. (2018). Functional sequestration of microRNA-122 from Hepatitis C Virus by circular RNA sponges. RNA Biol. *15*, 1032–1039. https://doi.org/10.1080/15476286.2018.1435248.

61. Liu, X., Abraham, J.M., Cheng, Y., Wang, Z., Wang, Z., Zhang, G., Ashktorab, H., Smoot, D.T., Cole, R.N., Boronina, T.N., et al. (2018). Synthetic Circular RNA Functions as a miR-21 Sponge to Suppress Gastric Carcinoma Cell Proliferation. Mol. Ther. Nucleic Acids *13*, 312–321. https://doi.org/10.1016/j.omtn.2018.09.010.

62. Liu, C.-X., Li, X., Nan, F., Jiang, S., Gao, X., Guo, S.-K., Xue, W., Cui, Y., Dong, K., Ding, H., et al. (2019). Structure and Degradation of Circular RNAs Regulate PKR Activation in Innate Immunity. Cell *177*, 865–880.e21. https://doi.org/10.1016/j.cell.2019.03.046.

63. Qu, L., Yi, Z., Shen, Y., Lin, L., Chen, F., Xu, Y., Wu, Z., Tang, H., Zhang, X., Tian, F., et al. (2022). Circular RNA vaccines against SARS-CoV-2 and emerging variants. Cell *185*, 1728–1744.e16. https://doi.org/10.1016/j.cell.2022.03.044.

64. Liu, B., Dong, X., Cheng, H., Zheng, C., Chen, Z., Rodríguez, T.C., Liang, S.-Q., Xue, W., and Sontheimer, E.J. (2022). A split prime editor with untethered reverse transcriptase and circular RNA template. Nat. Biotechnol. *40*, 1388–1393. https://doi.org/10.1038/s41587-022-01255-9.

65. Enuka, Y., Lauriola, M., Feldman, M.E., Sas-Chen, A., Ulitsky, I., and Yarden, Y. (2016). Circular RNAs are long-lived and display only minimal early alterations in response to a growth factor. Nucleic Acids Res. *44*, 1370–1383. https://doi.org/10.1093/nar/gkv1367.

66. Wesselhoeft, R.A., Kowalski, P.S., Parker-Hale, F.C., Huang, Y., Bisaria, N., and Anderson, D.G. (2019). RNA Circularization Diminishes Immunogenicity and Can Extend Translation Duration In Vivo. Mol. Cell *74*, 508–520.e4. https://doi.org/10.1016/j.molcel.2019.02.015.

67. Liu, C.-X., and Chen, L.-L. (2022). Circular RNAs: Characterization, cellular roles, and applications. Cell *185*, 2016–2034. https://doi.org/10.1016/j.cell.2022.04.021.

68. Zhang, C., Yang, Y., Qi, T., Zhang, Y., Hou, L., Wei, J., Yang, J., Shi, L., Ong, S.-G., Wang, H., et al. (2023). Prediction of base editor off-targets by deep learning. Nat. Commun. *14*, 5358. https://doi.org/10.1038/s41467-023-41004-3.

69. Kim, D., Bae, S., Park, J., Kim, E., Kim, S., Yu, H.R., Hwang, J., Kim, J.-I., and Kim, J.-S. (2015). Digenome-seq: genome-wide profiling of CRISPR-Cas9 off-target effects in human cells. Nat. Methods *12*, 237–243. https://doi.org/10.1038/nmeth.3284.

70. Kim, D., Lim, K., Kim, S.-T., Yoon, S.H., Kim, K., Ryu, S.-M., and Kim, J.-S. (2017). Genome-wide target specificities of CRISPR RNA-guided programmable deaminases. Nat. Biotechnol. *35*, 475–480. https://doi.org/10.1038/nbt.3852.

71. Tsai, S.Q., Zheng, Z., Nguyen, N.T., Liebers, M., Topkar, V.V., Thapar, V., Wyvekens, N., Khayter, C., Iafrate, A.J., Le, L.P., et al. (2015). GUIDE-Seq enables genome-wide profiling of off-target cleavage by CRISPR-Cas nucleases. Nat. Biotechnol. *33*, 187–197. https://doi.org/10.1038/nbt.3117.

72. Lei, Z., Meng, H., Lv, Z., Liu, M., Zhao, H., Wu, H., Zhang, X., Liu, L., Zhuang, Y., Yin, K., et al. (2021). Detect-seq reveals out-of-protospacer editing and target-strand editing by cytosine base editors. Nat. Methods *18*, 643–651. https://doi.org/10.1038/s41592-021-01172-w.

73. Yu, Y., Leete, T.C., Born, D.A., Young, L., Barrera, L.A., Lee, S.-J., Rees, H.A., Ciaramella, G., and Gaudelli, N.M. (2020). Cytosine base editors with minimized unguided DNA and RNA off-target events and high on-target activity. Nat. Commun. *11*, 2052. https://doi.org/10.1038/s41467-020-15887-5.

74. Doman, J.L., Raguram, A., Newby, G.A., and Liu, D.R. (2020). Evaluation and minimization of Cas9-independent off-target DNA editing by cytosine base editors. Nat. Biotechnol. *38*, 620–628. https://doi.org/10.1038/s41587-020-0414-6.

75. Rees, H.A., Komor, A.C., Yeh, W.-H., Caetano-Lopes, J., Warman, M., Edge, A.S.B., and Liu, D.R. (2017). Improving the DNA specificity and applicability of base editing through protein engineering and protein delivery. Nat. Commun. *8*, 15790. https://doi.org/10.1038/ncomms15790.

76. Villiger, L., Rothgangl, T., Witzigmann, D., Oka, R., Lin, P.J.C., Qi, W., Janjuha, S., Berk, C., Ringnalda, F., Beattie, M.B., et al. (2021). In vivo cytidine base editing of hepatocytes without detectable off-target mutations in RNA and DNA. Nat. Biomed. Eng. *5*, 179–189. https://doi.org/10.1038/s41551-020-00671-z.

77. Zhang, Y., Yang, L., and Chen, L.-L. (2021). Characterization of Circular RNAs. Methods Mol. Biol. *2372*, 179–192. https://doi.org/10.1007/978-1-0716-1697-0_16.

78. Karikó, K., Buckstein, M., Ni, H., and Weissman, D. (2005). Suppression of RNA Recognition by Toll-like Receptors: The Impact of Nucleoside Modification and the Evolutionary Origin of RNA. Immunity *23*, 165–175. https://doi.org/10.1016/j.immuni.2005.06.008.

79. Karikó, K., Muramatsu, H., Welsh, F.A., Ludwig, J., Kato, H., Akira, S., and Weissman, D. (2008). Incorporation of Pseudouridine Into mRNA Yields Superior Nonimmunogenic Vector With Increased Translational Capacity and Biological Stability. Mol. Ther. *16*, 1833–1840. https://doi.org/10.1038/mt.2008.200.

80. Andries, O., Mc Cafferty, S., De Smedt, S.C., Weiss, R., Sanders, N.N., and Kitada, T. (2015). N1-methylpseudouridine-incorporated mRNA outperforms pseudouridine-incorporated mRNA by providing enhanced protein expression and reduced immunogenicity in mammalian cell lines and mice. J. Control Release *217*, 337–344. https://doi.org/10.1016/j.jconrel.2015.08.051.

81. Zhang, M., Ma, Z., Selliah, N., Weiss, G., Genin, A., Finkel, T.H., and Cron, R.Q. (2014). The impact of Nucleofection® on the activation state of primary human CD4 T cells. J. Immunol. Methods *408*, 123–131. https://doi.org/10.1016/j.jim.2014.05.014.